Letter

Majorana zero modes in twisted transition metal dichalcogenide homobilayers

Xun-Jiang Luo,[1] Wen-Xuan Qiu,[1] and Fengcheng Wu[1,2,*]
[1]*School of Physics and Technology, Wuhan University, Wuhan 430072, China*
[2]*Wuhan Institute of Quantum Technology, Wuhan 430206, China*

(Received 30 August 2023; revised 6 December 2023; accepted 11 December 2023; published 8 January 2024)

Semiconductor moiré superlattices provide a highly tunable platform to study the interplay between electron correlation and band topology. For example, the generalized Kane-Mele-Hubbard model can be simulated by topological moiré flat bands in twisted transition metal dichalcogenide homobilayers. In this system, we obtain the filling factor, twist angle, and electric field-dependent quantum phase diagrams with a plethora of phases, including the quantum spin Hall insulator, the in-plane antiferromagnetic state, the out-of-plane antiferromagnetic Chern insulator, the spin-polarized Chern insulator, the in-plane ferromagnetic state, and the 120° antiferromagnetic state. We predict that a gate-defined junction formed between the quantum spin Hall insulator phase with proximitized superconductivity and the magnetic phases with in-plane magnetization (either ferromagnetism or antiferromagnetism) can realize a one-dimensional topological superconductor with Majorana zero modes. Our proposal introduces semiconductor moiré homobilayers as an electrically tunable Majorana platform with no need for an external magnetic field.

DOI: 10.1103/PhysRevB.109.L041103

Introduction. Transition metal dichalcogenide (TMD) moiré systems have attracted great research interest [1–23], as they provide a highly tunable platform for studying electron correlation, band topology, as well as their interplay. Mott insulators, generalized Wigner crystals, and quantum anomalous Hall insulators were experimentally observed in TMD moiré heterobilayers [4–11]. Twisted TMD homobilayers were predicted to host intrinsic topological moiré bands that can simulate the generalized Kane-Mele model [2]. Recent optical and transport experiments reported the observation of not only integer but also fractional quantum anomalous Hall insulators in twisted bilayer $MoTe_2$ ($t MoTe_2$) [24–28]. Signatures of the integer quantum anomalous Hall insulator were also detected in twisted bilayer WSe_2 ($t WSe_2$) using scanning single-electron transistor microscopy [29]. These exciting experimental findings immediately stimulated extensive theoretical investigations [30–35].

An appealing feature of twisted TMD homobilayers is that they host rich quantum phase diagrams that are experimentally tunable [24–29]. This is illustrated in Figs. 1(b) and 1(c), which show, respectively, our theoretical phase diagrams of $t WSe_2$ at hole filling factors $\nu_h = 2$ and $\nu_h = 1$ as functions of the twist angle θ and vertical electric-field-induced potential V_z. Here, the results are obtained by a mean-field study of a generalized Kane-Mele-Hubbard model. At $\nu_h = 2$, the theoretical phase diagram includes the quantum spin Hall insulator (QSHI), the in-plane antiferromagnetic state (AFM_x), the out-of-plane antiferromagnetic Chern insulator (AFM_z CI) with a Chern number C of 1, and the band insulator (BI). At $\nu_h = 1$, the theoretical phase diagram hosts the spin-polarized Chern insulator (CI) with $C = 1$, the topologically trivial out-of-plane ferromagnetic state (FM_z), the in-plane ferromagnetic state (FM_x), and the 120° antiferromagnetic state (120° AFM_{xy}). The phase transition between CI and topologically trivial magnetic insulators driven by V_z has recently been experimentally realized in both $t WSe_2$ and $t MoTe_2$ at $\nu_h = 1$ [24–29]. Since multiple phases can be realized within one system of a given θ by tuning ν_h and V_z, it is a promising direction to explore new physics that can emerge in junctions formed between different phases.

In this Letter, we theoretically predict that a planar junction formed between the QSHI phase with proximitized superconductivity (SC-QSHI) and the magnetic phases with in-plane magnetization (e.g., FM_x and AFM_x phases) can realize a one-dimensional (1D) topological superconductor (TSC) with Majorana zero modes (MZMs) at the boundaries, as illustrated in Figs. 1(e) and 1(f). The MZMs are highly sought after due to their non-Abelian braiding statistics and potential application in topological quantum computation [36]. Although MZMs are actively studied in several condensed matter platforms such as semiconductor nanowires [37–41], superconducting vortex cores in topological insulators [42–46], and ferromagnetic atomic chains [47,48], the deterministic evidence of MZMs is still an ongoing research topic. Therefore, it is worthwhile to search for new platforms to realize MZMs. Our theoretical proposal introduces TMD moiré systems as a potential Majorana platform based on two-dimensional materials [49–51], where MZMs can be tuned electrically without the need of any external magnetic field.

Model Hamiltonian and phase diagrams. We start with the generalized Kane-Mele-Hubbard model that can phenomenologically capture the interacting physics in topological bands of twisted TMD homobilayers [2],

$$H = H_{\rm KM} + U \sum_{i,\alpha} \hat{n}_{i\alpha\uparrow}\hat{n}_{i\alpha\downarrow} + \frac{V_z}{2}\sum_{i,\alpha} \ell_\alpha \hat{n}_{i\alpha}. \tag{1}$$

*wufcheng@whu.edu.cn

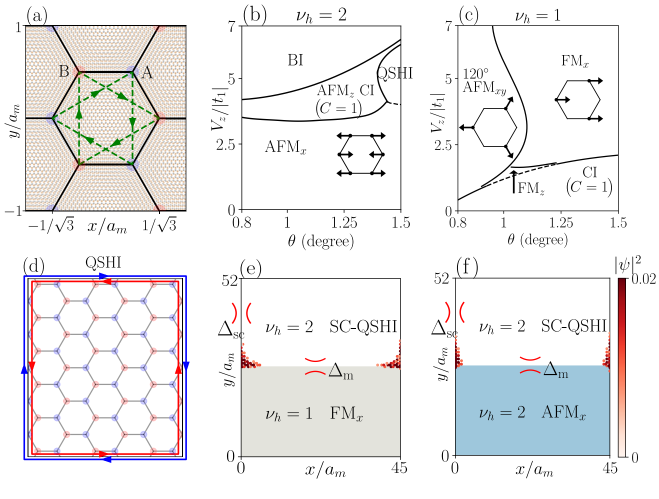

FIG. 1. (a) Illustration of the generalized Kane-Mele model on the effective honeycomb lattice formed in twisted TMD homobilayers. a_m is the moiré lattice constant. The green arrows denote the complex next-nearest-neighbor hopping. (b), (c) Quantum phase diagrams at $\nu_h = 2$ and $\nu_h = 1$, respectively. The solid (dashed) black lines mark the first-order (continuous) phase transition. The arrows on the honeycomb lattices represent the spin configuration. (d) Schematic illustration of the QSHI state. (e), (f) Spatial distribution of two MZMs in SC-QSHI/AFM$_x$ and SC-QSHI/FM$_x$ junctions, respectively. In (e) and (f), model parameters are fixed at the green points in Figs. 2(b) and 4(b), respectively.

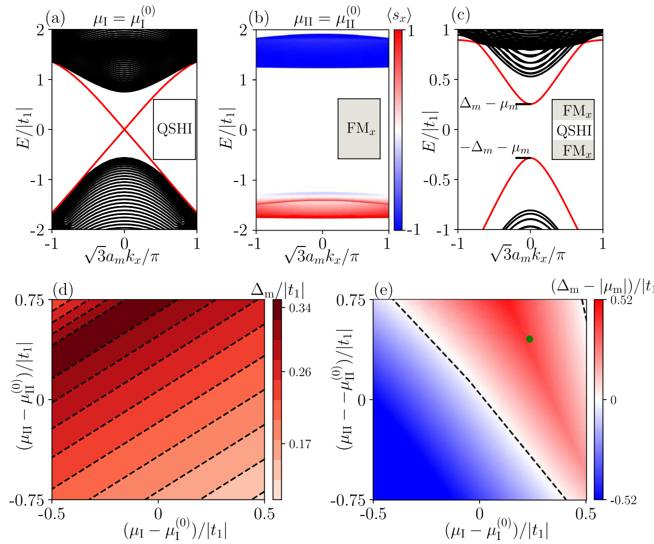

FIG. 2. (a), (b) Energy spectra of QSHI and FM$_x$ states in a cylinder geometry. In (a), the chemical potential $\mu_{\rm I}^{(0)}$ is taken to set the Dirac point of edge states (red lines) to be at zero energy. In (b), the chemical potential $\mu_{\rm II}^{(0)}$ is taken to set the middle of the charge gap to be at zero energy. (c) Energy spectra in a cylinder geometry for FM$_x$/QSHI/FM$_x$ junction. $2\Delta_m$ and μ_m denote the gap and effective chemical potential of the edge states, respectively. (d), (e) Numerical results of Δ_m and $\Delta_m - |\mu_m|$ as functions of $\mu_{\rm I}$ and $\mu_{\rm II}$. In (e), $\Delta_m - |\mu_m| = 0$ along the black dashed lines. In (c), parameters $\mu_{\rm I}$ and $\mu_{\rm II}$ are fixed at the green point in (e).

Here, $H_{\rm KM}$ is the generalized Kane-Mele Hamiltonian,

$$H_{\rm KM} = t_1 \sum_{\langle ij\rangle,\alpha\neq\beta,s} c_{i\alpha s}^\dagger c_{j\beta s} + |t_2| \sum_{\langle\langle ij\rangle\rangle,\alpha,s} e^{i\phi s\epsilon_{ij}} c_{i\alpha s}^\dagger c_{j\alpha s} + \cdots, \quad (2)$$

where subscripts α and β denote the A or B sublattice in the honeycomb lattice [Fig. 1(a)], s is the spin index that is locked to the valley index in TMDs, t_1 (t_2) is the hopping parameter between the nearest- (next-nearest-) neighbor sites, and the symbol $\cdots$ contains longer-range hopping terms. The next-nearest-neighbor hopping parameters carry spin- and sublattice-dependent phase factors $e^{i\phi s\epsilon_{ij}}$, where $s = +1$ (-1) for spin up (down) and $\epsilon_{ij} = \pm 1$ for different hopping paths [Fig. 1(a)]. In Eq. (1), U represents the on-site Hubbard repulsion, while the last term is a staggered sublattice potential $\ell_\alpha V_z/2$ with $\ell_{\rm A} = 1$ and $\ell_{\rm B} = -1$. This staggered potential is generated by an applied vertical electric field since the two sublattices are polarized to opposite layers [2]. The hopping parameters are tuned by the twist angle θ. Throughout this Letter, we use the hopping parameters derived for tWSe$_2$ [14,52], while the obtained results are also applicable to tMoTe$_2$.

We present the mean-field phase diagrams at $\nu_h = 2$ and $\nu_h = 1$ as functions of θ and V_z at $U = 5|t_1|$ in Figs. 1(b) and 1(c), respectively. Here, a phenomenological value of U is chosen to realize interaction-driven phases. At $\nu_h = 2$, the system with $V_z = 0$ would be in the QSHI phase in the noninteracting limit ($U = 0$) but is driven to the AFM$_x$ phase by a finite Hubbard repulsion U. Remarkably, the QSHI phase can reemerge in the presence of a finite V_z [Fig. 1(b)]. In addition, the AFM$_z$ CI phase can also be stabilized by the V_z field. The system is finally turned into a band insulator by a sufficiently large V_z. We note that all these four phases were previously reported for the Kane-Mele-Hubbard model [53]. At $\nu_h = 1$, the system is in the topologically nontrivial CI phase at small V_z but is driven to the topologically trivial magnetic phases (including FM$_z$, FM$_x$, and 120° AFM$_{xy}$ states) by large V_z. This V_z-tuned topological phase transition was recently experimentally observed [24–29]. Similar theoretical phase diagrams at $\nu_h = 1$ can be found in Refs. [14,54]. Since multiple phases can be stabilized by tuning V_z and ν_h at a fixed twist angle θ, electric gate-defined junctions formed between different quantum phases can be experimentally realized within one sample. In the following, we study junctions formed between the $\nu_h = 2$ QSHI phase and magnetic phases with in-plane magnetization such as $\nu_h = 1$ FM$_x$ and $\nu_h = 2$ AFM$_x$ phases.

Magnetic proximity effect. To study the QSHI/FM$_x$ junction, without loss of generality, we take $\theta = 1.5°$ and $V_z = 4|t_1|$, where the system is in the QSHI phase at $\nu_h = 2$ [Fig. 1(b)] and the FM$_x$ phase at $\nu_h = 1$ [Fig. 1(c)], respectively. We first characterize the two phases separately. The QSHI phase can be described by the mean-field Hamiltonian,

$$H_{\rm MF}^{\rm I} = H_{\rm KM} + \sum_{i,\alpha} \left(\frac{V_z \ell_\alpha + U \langle \hat{n}_{i\alpha} \rangle}{2} - \mu_{\rm I} \right) \hat{n}_{i\alpha}, \quad (3)$$

where $\langle \hat{n}_{i\alpha} \rangle$ is the mean-field average value of density operator $\hat{n}_{i\alpha}$ and $\mu_{\rm I}$ is the chemical potential. In Fig. 2(a), we present the energy spectra of $H_{\rm MF}^{\rm I}$ in a cylinder geometry with a periodic boundary condition along the x direction (armchair direction) and an open boundary condition along the y direction (zigzag direction). The red bands in Fig. 2(a) highlight the gapless helical edge states protected by time-reversal symmetry.

Similarly, the mean-field Hamiltonian for the FM_x phase is

$$H_{\mathrm{MF}}^{\mathrm{II}} = H_{\mathrm{KM}} + \sum_{i,\alpha}\left(\frac{V_z\ell_\alpha + U\langle\hat{n}_{i\alpha}\rangle}{2} - \mu_{\mathrm{II}}\right)\hat{n}_{i\alpha} - \frac{U}{2}\sum_{i,\alpha}\langle\hat{S}^x_{i\alpha}\rangle\hat{S}^x_{i\alpha}, \tag{4}$$

where $\hat{S}^x_{i\alpha} = \sum_{ss'} c^\dagger_{i\alpha s}(s_x)_{ss'}c_{i\alpha s'}$ with s_x being the Pauli matrix in the spin space and μ_{II} is the chemical potential. In Fig. 2(b), we plot the energy spectra of $H_{\mathrm{MF}}^{\mathrm{II}}$ in a cylinder geometry, which shows a sizable charge gap at $\nu_h = 1$. The color of the bands encodes the in-plane spin expectation value $\langle s_x\rangle$. The bands above the gap have larger $|\langle s_x\rangle|$ than that of bands right below the gap, because the former (latter) states mainly reside in the A (B) sites, and magnetic moments mainly develop at the A sites for $V_z > 0$. The interaction-driven magnetic term can be approximated as $-U\langle\hat{S}^x_{i\alpha}\rangle(\sigma_0+\sigma_z)s_x/4$ with the Pauli matrix σ_z acting in sublattice space.

We now study a symmetric FM_x/QSHI/FM_x junction with the junction interface along the armchair direction. We take the chemical potentials μ_{I} and μ_{II} for the two phases as independently tunable parameters and choose them such that zero energy is always within the bulk charge gap of each phase. The energy spectra of the junction in the cylinder geometry are shown in Fig. 2(c). The edge states of QSHI become gapped by the magnetic proximity effect. From the spectrum, we define $2\Delta_m$ as the gap and μ_m as the effective chemical potential of the edge states.

To have a qualitative understanding, we consider the spinor part of the armchair edge states $\Psi_{1,2}(y)$ of the QSHI for the semi-infinite system with $y > 0$, which generally takes the form [55]

$$\chi_1 = |\sigma_y = 1\rangle \otimes |s_z = -1\rangle,$$
$$\chi_2 = |\sigma_y = -1\rangle \otimes |s_z = 1\rangle. \tag{5}$$

Therefore, the two edge states $\Psi_{1,2}$ can be coupled by the sublattice-dependent magnetic term $-U\langle\hat{S}^x_{i\alpha}\rangle(\sigma_0+\sigma_z)s_x/4$, but not by a sublattice-independent term [55,56]. We note that an out-of-plane magnetic term cannot gap out the edge states, which is the reason to use magnetic phases with in-plane magnetization in the junction.

We present the numerical value of Δ_m as a function of μ_{I} and μ_{II} in Fig. 2(d). Here, Δ_m depends only on the difference $\mu_{\mathrm{II}} - \mu_{\mathrm{I}}$. We find that Δ_m becomes larger (smaller) as the QSHI edge state is tuned in energy closer to the conduction (valence) bands of the FM_x phase, which is consistent with the band-dependent magnetization shown in Fig. 2(b). In Fig. 2(e), we present the numerical value of $\Delta_m - |\mu_m|$ as a function of μ_{I} and μ_{II}. When $\Delta_m > |\mu_m|$, there are no states at the Fermi level and the system behaves as an insulator, which is important to realize MZMs as we will explain; otherwise, the system behaves as a metal.

MZMs in SC-QSHI/FM_x junction. We turn to study the SC-QSHI/FM_x junction, where the QSHI region has a proximitized superconducting pairing potential $\Delta_{\mathrm{sc}}\sum_{i\alpha} c^\dagger_{i\alpha\uparrow}c^\dagger_{i\alpha\downarrow}$ + H.c. This junction can be viewed as a 1D system with translational symmetry along the interface direction, which belongs to the D symmetry class of the Atland-Zirnbauer classification and can be characterized by the Z_2 topological invariant ξ if its energy spectra are fully gapped. Here, ξ can be defined by the Pfaffian value of the Hamiltonian of the system in the Majorana basis [57], and $\xi = -1$ (1) corresponds to a topological (trivial) phase with (without) robust MZMs at the boundary.

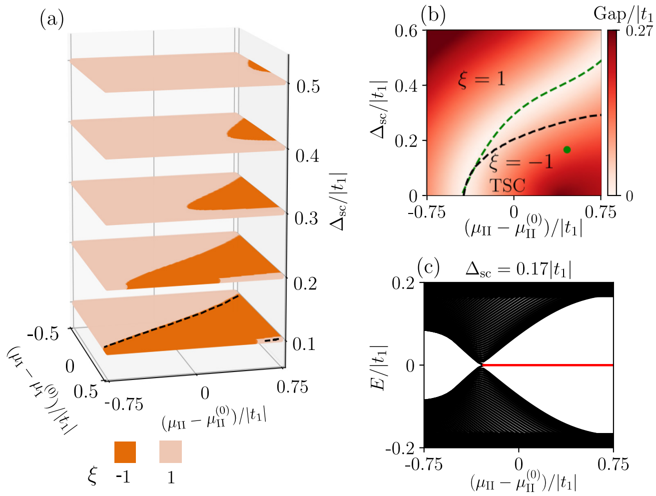

FIG. 3. Results for the the SC-QSHI/FM_x junction. (a) The phase diagram characterized by the Z_2 topological invariant ξ in a cylinder geometry as a function of μ_{I}, μ_{II}, and Δ_{sc}. (b) The energy gap in a cylinder geometry as a function of μ_{II} and Δ_{sc} at a fixed μ_{I}. The green dashed line marks the topological phase transition and the black dashed line is obtained through the effective edge theory of Eq. (6). (c) The energy spectra under open boundary conditions in both directions with respect to μ_{II} at fixed μ_{I} and Δ_{sc}. The red bands label the MZMs. In (b) and (c), μ_{I} takes the same value as that in Fig. 2(c).

We present the topological phase diagrams of the junction in a cylinder geometry as a function of μ_{I}, μ_{II}, and Δ_{sc} in Fig. 3(a). The phase diagrams can be understood as follows. In the parameter space where $\Delta_m > |\mu_m|$ (enclosed by the black dashed lines), an infinitesimal (but nonzero) pairing potential Δ_{sc} can drive this system into a TSC. This can be understood by examining a system with open boundary conditions in both directions, where the armchair and zigzag edges of QSHI have a magnetic-dominated gap and superconducting-dominated gap, respectively. In this case, there are isolated MZMs [58] at the ends of the interface in the SC-QSHI/FM_x junction [Fig. 1(e)]. The TSC region becomes narrower with increasing Δ_{sc} [Fig. 3(a)], which can be attributed to the gap closing at the junction interface. This topological phase transition can be revealed by the low-energy effective Hamiltonian of the armchair edge states

$$\tilde{\mathcal{H}} = k_x\tau_0 s_z + \Delta_m\tau_z s_x - \mu_m\tau_z s_0 + \tilde{\Delta}_{\mathrm{sc}}\tau_y s_y, \tag{6}$$

where the Pauli matrices $\tau_{y,z}$ act on the particle-hole (Nambu) space and $\tilde{\Delta}_{\mathrm{sc}}$ is the effective pairing potential for the edge states. The energy spectrum of $\tilde{\mathcal{H}}$ is closed when

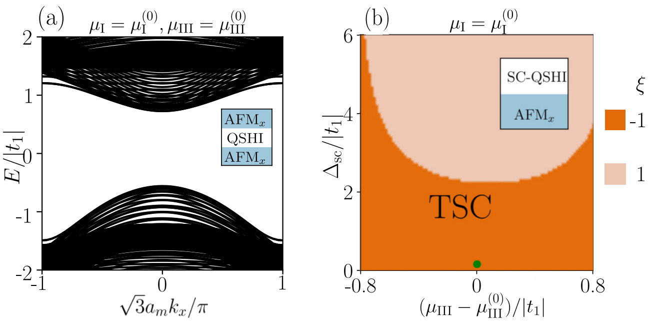

FIG. 4. (a) The energy spectra of the AFM$_x$/QSHI/AFM$_x$ junction (inset plots) in a cylinder geometry. (b) Topological phase diagram as a function of $\mu_{\rm III}$ and $\Delta_{\rm sc}$ for the SC-QSHI/AFM$_x$ junction in a cylinder geometry. $\mu_{\rm III}^{(0)}$ is taken to set the middle of the charge gap of the AFM$_x$ state to be at zero energy. In (a) and (b), we use $\theta = 1.5^\circ$ and $V_z = 2.5|t_1|$ for the AFM$_x$ state.

$\tilde{\Delta}_{\rm sc} = \sqrt{\Delta_m^2 - \mu_m^2}$, which is associated with a topological phase transition.

We present the numerical value of the energy gap of the junction in a cylinder geometry as a function of $\Delta_{\rm sc}$ and $\mu_{\rm II}$ at a fixed $\mu_{\rm I}$ in Fig. 3(b). The green dashed line characterizes the topological phase transition associated with the gap closing. The black dashed line plots $\tilde{\Delta}_{\rm sc} = \sqrt{\Delta_m^2 - \mu_m^2}$. The deviation between the two lines implies that the effective pairing potential $\tilde{\Delta}_{\rm sc}$ is smaller than $\Delta_{\rm sc}$. This is because the magnetic proximity effect suppresses the superconducting pairing for the edge states. To further elaborate on the topological phase transition, we present the open boundary energy spectra as a function of $\mu_{\rm II}$ at fixed $\mu_{\rm I}$ and $\Delta_{\rm sc}$ in Fig. 3(c), where the red bands represent the MZMs.

MZMs in SC-QSHI/AFM$_x$ junction. We now show that MZMs can also be realized by constructing the SC-QSHI/AFM$_x$ junction. The $\nu_h = 2$ AFM$_x$ state can also be described by the mean-field Hamiltonian in Eq. (4) but with $\langle \hat{S}^x_{i\rm A}\rangle = -\langle \hat{S}^x_{i\rm B}\rangle$, leading to the magnetic term $-U\langle \hat{S}^x_{i\rm A}\rangle \sigma_z s_x/2$. This term can gap the armchair edge states of QSHI described by Eq. (5). In Fig. 4(a), we plot the energy spectra of the AFM$_x$/QSHI/AFM$_x$ junction in a cylinder geometry, which are fully gapped as expected.

When adding the superconducting pairing potential to the QSHI phase, we obtain the SC-QSHI/AFM$_x$ junction, as shown in the inset of Fig. 4(b). Similar to the SC-QSHI/FM$_x$ junction, there are two robust MZMs at the ends of the interface of the SC-QSHI/AFM$_x$ junction [Fig. 1(f)]. In Fig. 4(b), we present the phase diagram as a function of $\mu_{\rm III}$ (i.e., the chemical potential in AFM$_x$ region) and $\Delta_{\rm sc}$ at fixed $\mu_{\rm I}$. We find that the TSC phase is relatively robust with respect to the variations of $\mu_{\rm III}$ and $\Delta_{\rm sc}$ [Fig. 4(b)]. This stability can be traced to the large magnetic energy gap opened by the magnetic proximity effect in the QSHI/AFM$_x$ junction.

Discussion. In summary, we introduce twisted TMD homobilayers as a potential platform to realize MZMs. The key of our proposal is to achieve gate-defined QSHI/FM$_x$ and QSHI/AFM$_x$ junctions, which is feasible because of the gate-tunable phase diagram and the recent experimental advances in nanodevice fabrication [59]. When bringing in the superconducting proximity effect for the QSHI state, the system can be topologically nontrivial and host MZMs, which can be detected, for example, by tunneling experiments through zero-bias conductance peaks [60]. Topological phase transitions can be readily tuned electrically without involving any external magnetic field, which is a potential advantage of our scheme.

The MZMs are protected by particle-hole symmetry and cannot be removed as long as the energy gap of the system persists. We use junctions with the interface along the armchair direction for illustration, but we find that MZMs can be realized for any generic interface direction [52]. In the calculation, the superconducting pairing potential is assumed to be uniform across the QSHI region and identical for the A and B sublattices. This assumption can be relaxed, since the main physics is governed by the edge states [52]. While we demonstrate that the TSC phase diagram is electrically tunable by adjusting the chemical potentials within the bulk charge gap, the parameter V_z can also serve as a tuning knob. In the search for MZMs, disorder effects often cannot be ignored [61]. The effect of disorder and interaction physics beyond mean-field theory in our scheme requires future study.

A fractional quantum anomalous Hall effect was recently observed in tMoTe$_2$ [25–28]. In contrast to Landau levels formed in an external magnetic field, twisted TMD homobilayers respect time-reversal symmetry, unless it is spontaneously broken, for example, in the (fractional) quantum anomalous Hall states. As a theoretical possibility, time-reversal symmetric fractional quantum spin Hall insulators [62,63] could also emerge in twisted TMD homobilayers. In the junctions studied in this Letter, parafermionic zero modes [64,65] can be realized when the QSHI state is replaced by its fractionalized cousins (i.e., the fractional quantum spin Hall insulators).

Acknowledgments. We thank Haining Pan, Chun-Xiao Liu, and Jie Wang for helpful discussion. This work is supported by National Natural Science Foundation of China (Grant No. 12274333), National Key Research and Development Program of China (Grants No. 2022YFA1402401 and No. 2021YFA1401300), and start-up funding of Wuhan University. We also acknowledge support by Key Research and Development Program of Hubei Province (Grant No. 2022BAA017). The numerical calculations in this paper have been performed on the supercomputing system in the Supercomputing Center of Wuhan University.

[1] F. Wu, T. Lovorn, E. Tutuc, and A. H. MacDonald, Hubbard model physics in transition metal dichalcogenide moiré bands, Phys. Rev. Lett. **121**, 026402 (2018).

[2] F. Wu, T. Lovorn, E. Tutuc, I. Martin, and A. H. MacDonald, Topological insulators in twisted transition metal dichalcogenide homobilayers, Phys. Rev. Lett. **122**, 086402 (2019).

[3] M. H. Naik and M. Jain, Ultraflatbands and shear solitons in moiré patterns of twisted bilayer transition metal dichalcogenides, Phys. Rev. Lett. **121**, 266401 (2018).
[4] L. Wang, E.-M. Shih, A. Ghiotto, L. Xian, D. A. Rhodes, C. Tan, M. Claassen, D. M. Kennes, Y. Bai, B. Kim, K. Watanabe, T. Taniguchi, X. Zhu, J. Hone, A. Rubio, A. N. Pasupathy, and C. R. Dean, Correlated electronic phases in twisted bilayer transition metal dichalcogenides, Nat. Mater. **19**, 861 (2020).
[5] Y. Tang, L. Li, T. Li, Y. Xu, S. Liu, K. Barmak, K. Watanabe, T. Taniguchi, A. H. MacDonald, J. Shan, and K. F. Mak, Simulation of Hubbard model physics in WSe_2/WS_2 moiré superlattices, Nature (London) **579**, 353 (2020).
[6] E. C. Regan, D. Wang, C. Jin, M. I. Bakti Utama, B. Gao, X. Wei, S. Zhao, W. Zhao, Z. Zhang, K. Yumigeta, M. Blei, J. D. Carlström, K. Watanabe, T. Taniguchi, S. Tongay, M. Crommie, A. Zettl, and F. Wang, Mott and generalized Wigner crystal states in WSe_2/WS_2 moiré superlattices, Nature (London) **579**, 359 (2020).
[7] Y. Xu, S. Liu, D. A. Rhodes, K. Watanabe, T. Taniguchi, J. Hone, V. Elser, K. F. Mak, and J. Shan, Correlated insulating states at fractional fillings of moiré superlattices, Nature (London) **587**, 214 (2020).
[8] H. Li, S. Li, E. C. Regan, D. Wang, W. Zhao, S. Kahn, K. Yumigeta, M. Blei, T. Taniguchi, K. Watanabe, S. Tongay, A. Zettl, M. F. Crommie, and F. Wang, Imaging two-dimensional generalized Wigner crystals, Nature (London) **597**, 650 (2021).
[9] T. Li, S. Jiang, B. Shen, Y. Zhang, L. Li, Z. Tao, T. Devakul, K. Watanabe, T. Taniguchi, L. Fu, J. Shan, and K. F. Mak, Quantum anomalous Hall effect from intertwined moiré bands, Nature (London) **600**, 641 (2021).
[10] M. Zhang, X. Zhao, K. Watanabe, T. Taniguchi, Z. Zhu, F. Wu, Y. Li, and Y. Xu, Tuning quantum phase transitions at half filling in 3L–$MoTe_2/WSe_2$ moiré superlattices, Phys. Rev. X **12**, 041015 (2022).
[11] W. Zhao, B. Shen, Z. Tao, Z. Han, K. Kang, K. Watanabe, T. Taniguchi, K. F. Mak, and J. Shan, Gate-tunable heavy fermions in a moiré Kondo lattice, Nature (London) **616**, 61 (2023).
[12] H. Pan, F. Wu, and S. Das Sarma, Band topology, Hubbard model, Heisenberg model, and Dzyaloshinskii-Moriya interaction in twisted bilayer WSe_2, Phys. Rev. Res. **2**, 033087 (2020).
[13] H. Pan, F. Wu, and S. Das Sarma, Quantum phase diagram of a Moiré-Hubbard model, Phys. Rev. B **102**, 201104(R) (2020).
[14] T. Devakul, V. Crépel, Y. Zhang, and L. Fu, Magic in twisted transition metal dichalcogenide bilayers, Nat. Commun. **12**, 6730 (2021).
[15] Y. Zhang, T. Devakul, and L. Fu, Spin-textured Chern bands in AB-stacked transition metal dichalcogenide bilayers, Proc. Natl. Acad. Sci. USA **118**, e2112673118 (2021).
[16] H. Pan, M. Xie, F. Wu, and S. Das Sarma, Topological phases in AB-stacked $MoTe_2/WSe_2$: Z_2 topological insulators, Chern insulators, and topological charge density waves, Phys. Rev. Lett. **129**, 056804 (2022).
[17] T. Devakul and L. Fu, Quantum anomalous Hall effect from inverted charge transfer gap, Phys. Rev. X **12**, 021031 (2022).
[18] Y.-M. Xie, C.-P. Zhang, J.-X. Hu, K. F. Mak, and K. T. Law, Valley-polarized quantum anomalous Hall state in moiré $MoTe_2/WSe_2$ heterobilayers, Phys. Rev. Lett. **128**, 026402 (2022).
[19] Y.-W. Chang and Y.-C. Chang, Quantum anomalous Hall effect and electric-field-induced topological phase transition in AB-stacked $MoTe_2/WSe_2$ moiré heterobilayers, Phys. Rev. B **106**, 245412 (2022).
[20] Z. Dong and Y.-H. Zhang, Excitonic Chern insulator and kinetic ferromagnetism in a $MoTe_2/WSe_2$ moiré bilayer, Phys. Rev. B **107**, L081101 (2023).
[21] Y.-M. Wu, Z. Wu, and H. Yao, Pair-density-wave and chiral superconductivity in twisted bilayer transition metal dichalcogenides, Phys. Rev. Lett. **130**, 126001 (2023).
[22] M. Xie, H. Pan, F. Wu, and S. Das Sarma, Nematic excitonic insulator in transition metal dichalcogenide moiré heterobilayers, Phys. Rev. Lett. **131**, 046402 (2023).
[23] X.-J. Luo, M. Wang, and F. Wu, Symmetric Wannier states and tight-binding model for quantum spin Hall bands in *AB*-stacked $MoTe_2/WSe_2$, Phys. Rev. B **107**, 235127 (2023).
[24] E. Anderson, F.-R. Fan, J. Cai, W. Holtzmann, T. Taniguchi, K. Watanabe, D. Xiao, W. Yao, and X. Xu, Programming correlated magnetic states with gate-controlled moiré geometry, Science **381**, 325 (2023).
[25] J. Cai, E. Anderson, C. Wang, X. Zhang, X. Liu, W. Holtzmann, Y. Zhang, F. Fan, T. Taniguchi, K. Watanabe, Y. Ran, T. Cao, L. Fu, D. Xiao, W. Yao, and X. Xu, Signatures of fractional quantum anomalous Hall states in twisted $MoTe_2$, Nature (London) **622**, 63 (2023).
[26] Y. Zeng, Z. Xia, K. Kang, J. Zhu, P. Knüppel, C. Vaswani, K. Watanabe, T. Taniguchi, K. F. Mak, and J. Shan, Thermodynamic evidence of fractional Chern insulator in moiré $MoTe_2$, Nature (London) **622**, 69 (2023).
[27] H. Park, J. Cai, E. Anderson, Y. Zhang, J. Zhu, X. Liu, C. Wang, W. Holtzmann, C. Hu, Z. Liu, T. Taniguchi, K. Watanabe, J.-H. Chu, T. Cao, L. Fu, W. Yao, C.-Z. Chang, D. Cobden, D. Xiao, and X. Xu, Observation of fractionally quantized anomalous Hall effect, Nature (London) **622**, 74 (2023).
[28] F. Xu, Z. Sun, T. Jia, C. Liu, C. Xu, C. Li, Y. Gu, K. Watanabe, T. Taniguchi, B. Tong, J. Jia, Z. Shi, S. Jiang, Y. Zhang, X. Liu, and T. Li, Observation of integer and fractional quantum anomalous Hall effects in twisted bilayer $MoTe_2$, Phys. Rev. X **13**, 031037 (2023).
[29] B. A. Foutty, C. R. Kometter, T. Devakul, A. P. Reddy, K. Watanabe, T. Taniguchi, L. Fu, and B. E. Feldman, Mapping twist-tuned multi-band topology in bilayer WSe_2, arXiv:2304.09808.
[30] C. Wang, X.-W. Zhang, X. Liu, Y. He, X. Xu, Y. Ran, T. Cao, and D. Xiao, Fractional Chern insulator in twisted bilayer $MoTe_2$, arXiv:2304.11864.
[31] A. P. Reddy, F. Alsallom, Y. Zhang, T. Devakul, and L. Fu, Fractional quantum anomalous Hall states in twisted bilayer $MoTe_2$ and WSe_2, Phys. Rev. B **108**, 085117 (2023).
[32] W.-X. Qiu, B. Li, X.-J. Luo, and F. Wu, Interaction-driven topological phase diagram of twisted bilayer $MoTe_2$, Phys. Rev. X **13**, 041026 (2023).
[33] J. Dong, J. Wang, P. J. Ledwith, A. Vishwanath, and D. E. Parker, Composite Fermi liquid at zero magnetic field in twisted $MoTe_2$, Phys. Rev. Lett. **131**, 136502 (2023).
[34] H. Goldman, A. P. Reddy, N. Paul, and L. Fu, Zero-field composite Fermi liquid in twisted semiconductor bilayers, Phys. Rev. Lett. **131**, 136501 (2023).
[35] N. Morales-Durán, N. Wei, and A. H. MacDonald, Magic angles and fractional Chern insulators in twisted homobilayer TMDs, arXiv:2308.03143.

[36] C. Nayak, S. H. Simon, A. Stern, M. Freedman, and S. Das Sarma, Non-Abelian anyons and topological quantum computation, Rev. Mod. Phys. **80**, 1083 (2008).

[37] J. D. Sau, R. M. Lutchyn, S. Tewari, and S. Das Sarma, Generic new platform for topological quantum computation using semiconductor heterostructures, Phys. Rev. Lett. **104**, 040502 (2010).

[38] R. M. Lutchyn, J. D. Sau, and S. Das Sarma, Majorana fermions and a topological phase transition in semiconductor-superconductor heterostructures, Phys. Rev. Lett. **105**, 077001 (2010).

[39] Y. Oreg, G. Refael, and F. von Oppen, Helical liquids and Majorana bound states in quantum wires, Phys. Rev. Lett. **105**, 177002 (2010).

[40] V. Mourik, K. Zuo, S. M. Frolov, S. R. Plissard, E. P. A. M. Bakkers, and L. P. Kouwenhoven, Signatures of Majorana fermions in hybrid superconductor-semiconductor nanowire devices, Science **336**, 1003 (2012).

[41] J. Alicea, New directions in the pursuit of Majorana fermions in solid state systems, Rep. Prog. Phys. **75**, 076501 (2012).

[42] L. Fu and C. L. Kane, Superconducting proximity effect and Majorana fermions at the surface of a topological insulator, Phys. Rev. Lett. **100**, 096407 (2008).

[43] H.-H. Sun, K.-W. Zhang, L.-H. Hu, C. Li, G.-Y. Wang, H.-Y. Ma, Z.-A. Xu, C.-L. Gao, D.-D. Guan, Y.-Y. Li, C. Liu, D. Qian, Y. Zhou, L. Fu, S.-C. Li, F.-C. Zhang, and J.-F. Jia, Majorana zero mode detected with spin selective Andreev reflection in the vortex of a topological superconductor, Phys. Rev. Lett. **116**, 257003 (2016).

[44] G. Xu, B. Lian, P. Tang, X.-L. Qi, and S.-C. Zhang, Topological superconductivity on the surface of Fe-based superconductors, Phys. Rev. Lett. **117**, 047001 (2016).

[45] D. Wang, L. Kong, P. Fan, H. Chen, S. Zhu, W. Liu, L. Cao, Y. Sun, S. Du, J. Schneeloch, R. Zhong, G. Gu, L. Fu, H. Ding, and H.-J. Gao, Evidence for Majorana bound states in an iron-based superconductor, Science **362**, 333 (2018).

[46] A. Mercado, S. Sahoo, and M. Franz, High-temperature Majorana zero modes, Phys. Rev. Lett. **128**, 137002 (2022).

[47] S. Nadj-Perge, I. K. Drozdov, J. Li, H. Chen, S. Jeon, J. Seo, A. H. MacDonald, B. A. Bernevig, and A. Yazdani, Observation of Majorana fermions in ferromagnetic atomic chains on a superconductor, Science **346**, 602 (2014).

[48] S. Jeon, Y. Xie, J. Li, Z. Wang, B. A. Bernevig, and A. Yazdani, Distinguishing a Majorana zero mode using spin-resolved measurements, Science **358**, 772 (2017).

[49] P. San-Jose, J. L. Lado, R. Aguado, F. Guinea, and J. Fernández-Rossier, Majorana zero modes in graphene, Phys. Rev. X **5**, 041042 (2015).

[50] A. Thomson, I. M. Sorensen, S. Nadj-Perge, and J. Alicea, Gate-defined wires in twisted bilayer graphene: From electrical detection of intervalley coherence to internally engineered Majorana modes, Phys. Rev. B **105**, L081405 (2022).

[51] Y.-M. Xie, E. Lantagne-Hurtubise, A. F. Young, S. Nadj-Perge, and J. Alicea, Gate-defined topological Josephson junctions in Bernal bilayer graphene, Phys. Rev. Lett. **131**, 146601 (2023).

[52] See Supplemental Material at http://link.aps.org/supplemental/10.1103/PhysRevB.109.L041103 for a continuum model and tight-binding model for moiré bands, Hartree-Fock mean-field calculation, and additional phase diagrams.

[53] K. Jiang, S. Zhou, X. Dai, and Z. Wang, Antiferromagnetic Chern insulators in noncentrosymmetric systems, Phys. Rev. Lett. **120**, 157205 (2018).

[54] B. Li, W.-X. Qiu, and F. Wu, Electrically tuned topology and magnetism in twisted bilayer $MoTe_2$ at $\nu_h = 1$, arXiv:2310.02217.

[55] X.-H. Pan, K.-J. Yang, L. Chen, G. Xu, C.-X. Liu, and X. Liu, Lattice-symmetry-assisted second-order topological superconductors and Majorana patterns, Phys. Rev. Lett. **123**, 156801 (2019).

[56] Y. Ren, Z. Qiao, and Q. Niu, Engineering corner states from two-dimensional topological insulators, Phys. Rev. Lett. **124**, 166804 (2020).

[57] A. Y. Kitaev, Unpaired Majorana fermions in quantum wires, Phys. Usp. **44**, 131 (2001).

[58] L. Fu and C. L. Kane, Josephson current and noise at a superconductor/quantum-spin-Hall-insulator/superconductor junction, Phys. Rev. B **79**, 161408(R) (2009).

[59] J. Díez-Mérida, A. Díez-Carlón, S. Y. Yang, Y.-M. Xie, X.-J. Gao, J. Senior, K. Watanabe, T. Taniguchi, X. Lu, A. P. Higginbotham, K. T. Law, and D. K. Efetov, Symmetry-broken Josephson junctions and superconducting diodes in magic-angle twisted bilayer graphene, Nat. Commun. **14**, 2396 (2023).

[60] J. Liu, A. C. Potter, K. T. Law, and P. A. Lee, Zero-bias peaks in the tunneling conductance of spin-orbit-coupled superconducting wires with and without Majorana end-states, Phys. Rev. Lett. **109**, 267002 (2012).

[61] H. Pan and S. Das Sarma, Physical mechanisms for zero-bias conductance peaks in Majorana nanowires, Phys. Rev. Res. **2**, 013377 (2020).

[62] M. Levin and A. Stern, Fractional topological insulators, Phys. Rev. Lett. **103**, 196803 (2009).

[63] X.-L. Qi, Generic wave-function description of fractional quantum anomalous Hall states and fractional topological insulators, Phys. Rev. Lett. **107**, 126803 (2011).

[64] N. H. Lindner, E. Berg, G. Refael, and A. Stern, Fractionalizing Majorana fermions: Non-Abelian statistics on the edges of Abelian quantum Hall states, Phys. Rev. X **2**, 041002 (2012).

[65] D. J. Clarke, J. Alicea, and K. Shtengel, Exotic non-Abelian anyons from conventional fractional quantum Hall states, Nat. Commun. **4**, 1348 (2013).